Journal of Radiotherapy in Practice

cambridge.org/jrp

Evaluating small field dosimetry with the Acuros XB (AXB) and analytical anisotropic algorithm (AAA) dose calculation algorithms in the eclipse treatment planning system

Sepideh Behinaein[1], Ernest Osei[1,2,3,4], Johnson Darko[1,2,3], Paule Charland[1,2] and Dylan Bassi[2]

[1]Department of Medical Physics, Grand River Regional Cancer Centre, Kitchener, Canada; [2]Department of Physics and Astronomy, University of Waterloo, Waterloo, Canada; [3]Department of Clinical Studies, Ontario Veterinary College, University of Guelph, Guelph, Canada and [4]Department of Systems Design Engineering, University of Waterloo, Waterloo, Canada

Original Article

Cite this article: Behinaein S, Osei E, Darko J, Charland P, and Bassi D. (2019) Evaluating small field dosimetry with the Acuros XB (AXB) and analytical anisotropic algorithm (AAA) dose calculation algorithms in the eclipse treatment planning system. *Journal of Radiotherapy in Practice* **18**: 353–364. doi: 10.1017/S1460396919000104

Received: 29 November 2018
Revised: 19 January 2019
Accepted: 27 January 2019
First published online: 29 April 2019

Key words:
Acuros XB; analytical anisotropic algorithm; EGSnrc Monte Carlo simulation; Exradin W1 Scintillator measurement; small field dosimetry

Author for correspondence:
Ernest Osei, Grand River Regional Cancer Centre, 835 King Street West, Kitchener, Ontario N2G1G3, Canada. Tel: 519 749 4300 ext. 5407. E-mail: ernest.osei@grhosp.on.ca

Abstract

Background: An increasing number of external beam treatment modalities including intensity modulated radiation therapy, volumetric modulated arc therapy (VMAT) and stereotactic radiosurgery uses very small fields for treatment planning and delivery. However, there are major challenges in small photon field dosimetry, due to the partial occlusion of the direct photon beam source's view from the measurement point, lack of lateral charged particle equilibrium, steep dose-rate gradient and volume averaging effect of the detector response and variation of the energy fluence in the lateral direction of the beam. Therefore, experimental measurements of dosimetric parameters such as percent depth doses (PDDs), beam profiles and relative output factors (ROFs) for small fields continue to be a challenge.

Materials and Methods: In this study, we used a homogeneous water phantom and the heterogeneous anthropomorphic stereotactic end-to-end verification (STEEV) head phantom for all dose measurements and calculations. PDDs, lateral dose profiles and ROFs were calculated in the Eclipse Treatment Planning System version 13·6 using the Acuros XB (AXB) and the analytical anisotropic algorithms (AAAs) in a homogenous water phantom. Monte Carlo (MC) simulations and measurements using the Exradin W1 Scintillator were also accomplished for four photon energies: 6 MV, 6FFF, 10 MV and 10FFF. Two VMAT treatment plans were generated for two different targets: one located in the brain and the other in the neck (close to the trachea) in the head phantom (CIRS, Norfolk, VA, USA). A Varian Truebeam linear accelerator (Varian, Palo Alto, CA, USA) was used for all treatment deliveries. Calculated results with AXB and AAA were compared with MC simulations and measurements.

Results: The average difference of PDDs between W1 Exradin Scintillator measurements and MC simulations, AAA and AXB algorithm calculations were 1·2, 2·4 and 3·2%, respectively, for all field sizes and energies. AXB and AAA showed differences in ROF of about 0·3 and 2·9%, respectively, compared with W1 Exradin Scintillator measured values. For the target located in the brain in the head phantom, the average dose difference between W1 Exradin Scintillator and the MC simulations, AAA and AXB were 0·2, 3·2 and 2·7%, respectively, for all field sizes. Similarly, for the target located in the neck, the respective dose differences were 3·8, 5·7 and 3·5%.

Conclusion: In this study, we compared dosimetric parameters such as PDD, beam profile and ROFs in water phantom and isocenter point dose measurements in an anthropomorphic head phantom representing a patient. We observed that measurements using the W1 Exradin scintillator agreed well with MC simulations and can be used efficiently for dosimetric parameters such as PDDs and dose profiles and patient-specific quality assurance measurements for small fields. In both homogenous and heterogeneous media, the AXB algorithm dose prediction agrees well with MC and measurements and was found to be superior to the AAA algorithm.

Introduction

In external beam radiation therapy, beam apertures of 4×4 cm^2 to 40×40 cm^2 are commonly used in treatment planning and delivery.[1,2] However, with the advent of stereotactic radiosurgery (SRS), stereotactic body radiotherapy (SBRT), intensity modulated radiation therapy and volumetric modulated arc therapy (VMAT), smaller beam sizes (below 4×4 cm^2) are being used in treatment planning and delivery.[2] Nevertheless, there are major challenges in the small photon field dosimetry due to the partial occlusion of the direct photon beam source's view from the measurement point,[3] lack of lateral charged particle equilibrium, steep dose-rate gradient,

© Cambridge University Press 2019.

CAMBRIDGE UNIVERSITY PRESS

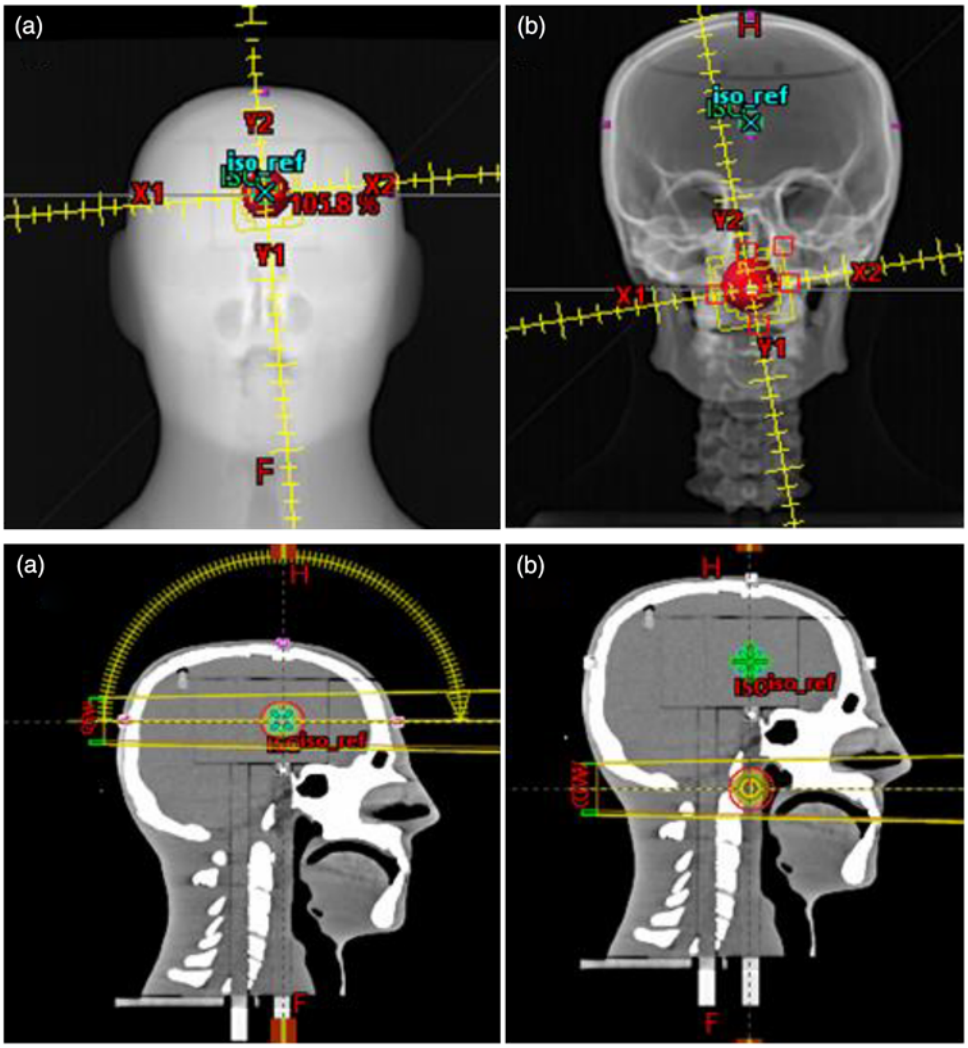


Figure 1. VMAT treatment plans for (a) the target located in the brain using one and half arcs and (b) the target located in the neck (close to the trachea) using 2 full arcs. This figure presents the target size of 3 cm in diameter in the stereotactic end-to-end verification (STEEV) head phantom.

volume averaging effect of the detector response and variation of the energy fluence in the lateral direction of the beam.[3–5] Consequently, the experimental measurements of dosimetric parameters such as percent depth doses (PDDs), beam profiles and output factors for small fields continue to be a challenge. Additionally, the accuracy of small field measurements is also highly dependent on the choice of the detector.

Several dosimeters have been used for small field dosimetry with varying challenges and limitations;[6] however, the ideal characteristics of a detector suitable for small field dosimetry are high resolution (small full width half maximum (FWHM)), water equivalent, linear response, energy and dose-rate independence.[6,7] Detectors that have been used in small fields dosimetry include small air ionisation chambers,[8,9] liquid ionisation chambers,[10–12] silicon diodes,[13] diamond detectors,[14] plastic and organic scintillators,[15] radiographic and radiochromic films,[16,17] metal oxide semiconductor field-effect transistors,[18] thermoluminescent dosimeters and optically stimulated luminescence detectors.[19] The International Atomic Energy Commission (IAEA)-Technical Report Series No. 482 (Technical Report Series (TRS) 483)[6] provides a comprehensive overview of the properties of detectors used in small field dosimetry and their limitations. According to Carrasco et al.,[7] the W1 Exradin plastic scintillator (Standard Imaging, Inc., Middleton, WI, USA) with the optimal characteristics including water equivalence, linear dose–response, dose-rate independence, energy independence in megavoltage (MV) range and high spatial resolution is an acceptable detector for measuring dosimetric parameters in small photon fields.

A significant limitation on the accuracy of the dose delivered to patients in radiation therapy depends on the accuracy of the treatment planning system (TPS) dose calculation algorithms. In the past few years, the desire to achieve accurate dose calculations in TPSs for small fields and heterogeneous media has necessitated the development of algorithms commensurate in calculation accuracy.[20] Dose calculation algorithms in TPSs are classified into either data-driven algorithms or model-driven algorithms or Monte Carlo (MC) simulation. Data-driven algorithms are based on the measured data and use simplified methods such as 'Modified Batho'[21] or 'Equivalent Tissue to Air Ratio'[22] to account for inhomogeneity and can greatly overestimate doses as much as 20% in areas where lateral electron disequilibrium exists such as the lung.[23] On the other hand, the model-driven algorithms [e.g., analytical anisotropic algorithm (AAA),[24] collapsed cone convolution (CCC) algorithm[25] and Acuros XB (AXB) algorithm[26]] are based on beam models which

https://doi.org/10.1017/S1460396919000104 Published online by Cambridge University Press

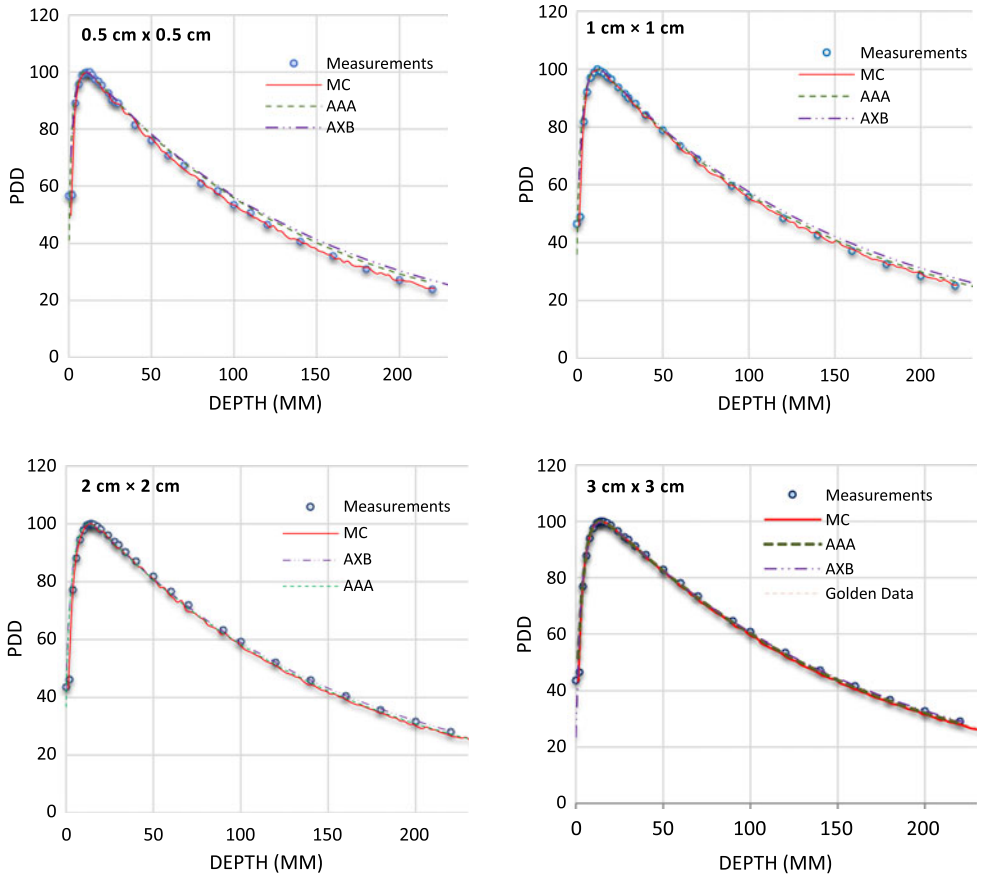


Figure 2. Percentage depth dose (PDD) profiles for 6 MV photon beams with field sizes ranging from 0·5 cm × 0·5 cm to 3 cm × 3 cm in a homogeneous water phantom comparing W1 Exradin scintillator measurements, Monte Carlo (MC) simulations and the calculation algorithms analytical anisotropic algorithm (AAA) and Acuros XB (AXB) in the eclipse treatment planning system. The Varian golden beam data are also included in the plot for a 3 cm × 3 cm field size.

may or may not have adjustable parameters. The model-driven algorithms are capable of modelling electron transport in an approximate or explicit manner. The AAA and CCC algorithms have been considered acceptable for conditions of moderate electron disequilibrium but errors as large as 8% have been reported for small fields with 18 MV in a lung phantom.[24] In comparison to the AAA and CCC algorithms, the AXB algorithm is capable of producing more accurate dose calculations within heterogeneous media.[27] The MC approach to dose calculations is generally considered the gold standard for determining dose distributions in any medium. It is known to give more accurate dosimetry in areas of electron disequilibrium, and where interpretations of dosimetric measurements are challenging. As such, it has been used by many authors to benchmark the accuracy of different dose calculation techniques.[28,29] Han et al.[27] showed less than 2% agreement when comparing dose distributions produced by the AXB algorithm and MC simulation for an 18 MV beam and 2·5 × 2·5 cm^2 field incident on a heterogeneous phantom.

A number of investigations[30–33] have been concerned with the validation and comparison of the relatively new AXB algorithm against measurements using various detectors, MC calculations, AAA algorithms or a combination of these modalities. However, few studies have evaluated the accuracy of the AXB algorithm against measurements using the W1 Exradin scintillator detector (Standard Imaging, Inc., Middleton, WI, USA) for small fields in a heterogeneous phantom.[33–35] Limited studies have investigated the accuracy of small field dosimetry with the AAA and AXB for field sizes as small as 1 × 1 cm^2.[34,35] In this study, we evaluated the accuracy of the AXB and AAA algorithms in the eclipse TPS (Varian Medical System, Palo Alto, CA, USA) version 13·6 for small radiation fields ranging from 0·5 × 0·5 cm^2 to 3 × 3 cm^2. Dosimetric parameters calculated from the TPS using the AXB and AAA algorithms are compared with phantom measurements using the W1 Exradin scintillator (Standard Imaging, Inc., Middleton, WI, USA) and simulated data using the EGSnrc MC code. The goal is to evaluate the dosimetric accuracy of the AXB and AAA dose calculation algorithms in the Eclipse TPS for small fields and to investigate the potential use of the W1 Exradin scintillator detector for patient-specific quality assurance measurements using an anthropomorphic head and neck phantom.

Materials and Methods

Dose calculations in Eclipse TPS

Commissioning beam data are treated as a reference and ultimately used by TPSs; therefore, it is extremely important that the data used are of the highest quality to avoid dosimetric and patient treatment errors that may subsequently lead to a poor radiation outcome. Our Truebeam linacs are matched to the Varian Golden Beam Data (GBD) and hence the commissioning data used for the beam configurations for both the AAA and AXB algorithms in the TPS are based on the GBD provided by the vendor. However, comprehensive measurements were done for validation during commissioning of both the TPS and Linacs using the Task

https://doi.org/10.1017/S1460396919000104 Published online by Cambridge University Press

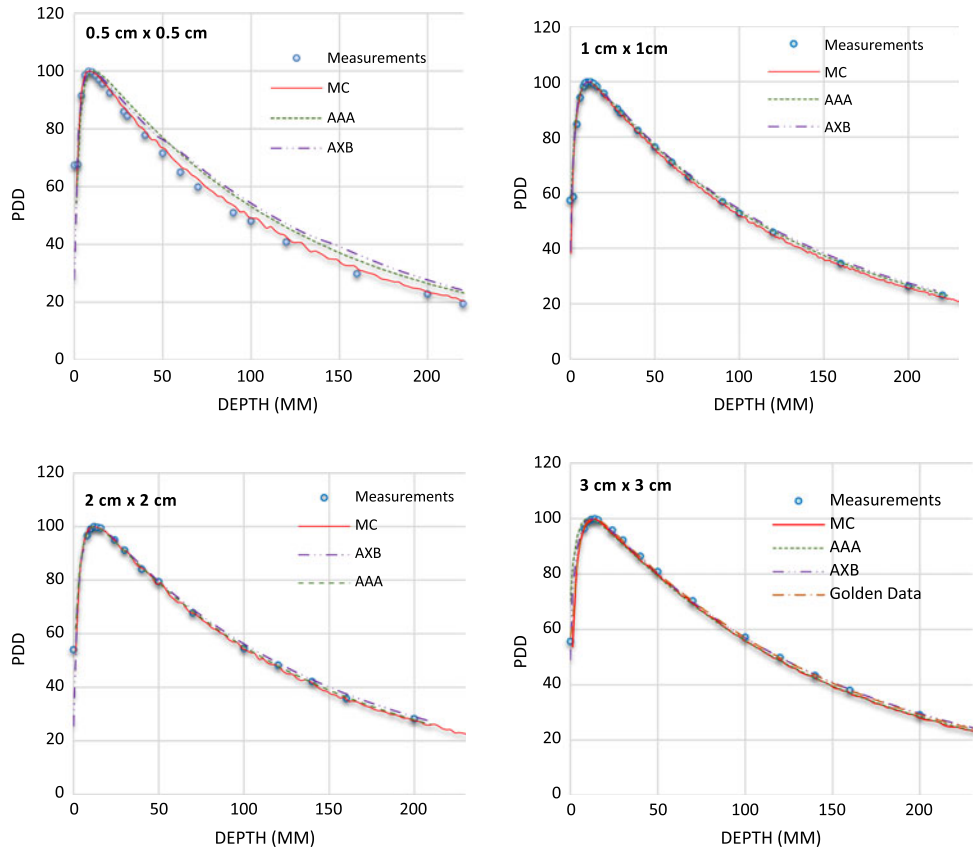


Figure 3. Percentage depth dose (PDD) profiles for 6 FFF MV photon beams with field sizes ranging from 0·5 cm × 0·5 cm to 3 cm × 3 cm in a homogeneous water phantom comparing W1 Exradin scintillator measurements, Monte Carlo (MC) simulations and the calculation algorithms analytical anisotropic algorithm (AAA) and Acuros XB (AXB) in the eclipse treatment planning system. The Varian golden beam data are also included in the plot for a 3 cm × 3 cm field size.

Group 106 (TG-106)[36] of the Therapy Physics Committee of the American Association of Physicists in Medicine (AAPM) guidelines and recommendations on the proper selection of phantoms and detectors, setting up of a phantom for data acquisition (both scanning and no-scanning data), procedures for acquiring specific photon and electron beam parameters and methods to reduce measurement errors, beam data processing and detector size convolution for accurate profiles.

We verified the golden beam input data by measuring machine's outputs, PDDs and profiles (in-plane and cross plane) at different depths in a water tank for various field sizes (ranging from 3 × 3 cm^2 to 40 × 40 cm^2) and all photon energies: 6 MV, 6FFF, 10 MV, 10FFF and 15 MV. We used the CC13 ionisation chamber (IBA Dosimetry GmbH, Schwarzenbruck, Germany) with active volume of 0·13 cm^3 and an IBA photon dosimetry diode detector with an active area diameter of 2 mm for profiles and small fields' measurements. We also created phantoms in the TPS and calculated doses for various geometries and energies and compared with measurements.

For this work, the AXB and AAA calculation algorithms in the Eclipse TPS (Varian Medical System, Palo Alto, CA, USA) were validated in a homogenous medium for 6 MV, 6FFF MV, 10 MV and 10FFF MV photon beam energies. Measurements and calculations were performed in a 30 × 30 × 30 cm^3 water equivalent phantom created in the TPS. The grid size used for the dose calculation was 1 × 1 × 1 mm^3. To investigate the dose distribution as a function of depth in the phantom, central axis (CAX) PDD curves were calculated in the water phantom using both AAA and AXB algorithms for field sizes from 0·5 × 0·5 cm^2 to 3 × 3 cm^2 at source-surface distance (SSD) = 100 cm. Relative output factors (ROFs) were evaluated for all field sizes and energies at the depth of 5 cm and SSD = 95 cm at CAX using both algorithms. The calculated point doses at the depth of 5 cm for each field size and energy were normalised to doses using 10 × 10 cm^2 field size. Beam profiles at a depth of 5 cm and SSD = 100 cm were calculated for all field sizes and beam energies. All dose calculations were performed using the Eclipse TPS version 13·6 (Varian Medical System, Palo Alto, CA, USA). The AXB algorithm uses the material composition for the voxels from a predefined material library.[37,38]

MC simulations

MC simulation is a computerised mathematical technique used to simulate photon transport based on the fundamental principles of radiation transport. The EGSnrc MC code including the user code DOSXYZnrc, which is a three-dimensional voxel dose calculation module, was used to carry out MC simulations of radiation transport through a water phantom with dimensions of 20 × 20 × 50 cm^3, a resolution of 2·5 × 2·5 × 2·5 mm^3 and a field size of 3 × 3 cm^2. For smaller field sizes of 0·5 × 0·5 cm^2 to 2 × 2 cm^2, a phantom with dimensions of 6 × 6 × 50 cm^3 and a resolution of 1 × 1 × 1 mm^3 was used. The MC code simulates the transport of each radiation particle in the given medium according to the probabilities or cross-sections of the allowed interactions. In this way, the path of each particle is traced until it is either absorbed or escapes from the phantom and the discrete energy deposition steps are accrued.

https://doi.org/10.1017/S1460396919000104 Published online by Cambridge University Press

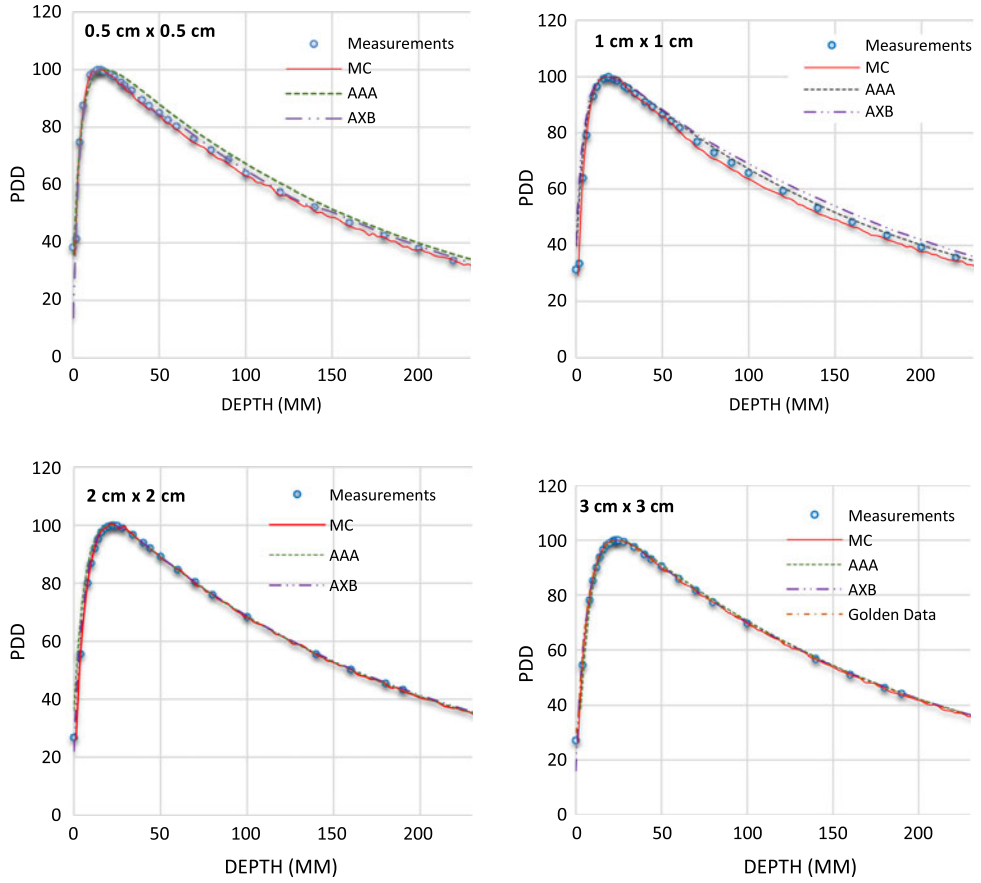


Figure 4. Percentage depth dose (PDD) profiles for 10 MV photon beams with field sizes ranging from 0·5 cm × 0·5 cm to 3 cm × 3 cm in a homogeneous water phantom comparing W1 Exradin scintillator measurements, Monte Carlo (MC) simulations and the calculation algorithms analytical anisotropic algorithm (AAA) and Acuros XB (AXB) in the eclipse treatment planning system. The Varian golden beam data are also included in the plot for a 3 cm × 3 cm field size.

The final dose distribution is the result of histories of accumulated energy deposition events. Depending on the field size, about 10^7 photon histories were used for each simulation and the values of the electron cut off energy (ECUT) and photon cut off energy (PCUT) transport cut-off energies used are 100 and 10 keV, respectively. The electron AE and photon AP production thresholds used were 10 keV. The accuracy of MC dose calculations will increase with decrease in voxel size; however, decreasing the voxel size will result in increase in statistical uncertainty in the dose calculations. Therefore, to improve the statistical accuracy will require increasing the number of photon histories simulated and hence increase in CPU time and computer memory.[29,39,40] The elemental composition of soft tissue used in the simulation is that of ICRU-44.[41] A realistic Varian linear accelerator was modelled as the source of radiation using data supplied by the manufacture (Varian Medical System, Palo Alto, CA, USA).

Experimental measurements

The Exradin W1 scintillator (Standard Imaging, Inc., Middleton, WI, USA) used in this study is a commercially available detector that contains a scintillating element with an active volume of 1 mm diameter by 3 mm length and an acrylic (Polymethyl methacrylate (PMMA)) optic fibre with 1 mm diameter core. The biggest concern for using the W1 Exradin scintillator is to account for the Cerenkov radiation produced in the transport optic fibre. When charged particles are travelling at a speed greater than the phase velocity of light, Cerenkov radiation is emitted in the form of visible light. The amount of Cerenkov radiation directly correlates with the length of optical fibre exposed in the radiation beam, and these signals act as noise and cause erroneously large readings if not corrected.[42] Guillot et al.[43] proposed a chromic removal method to remove the Cerenkov radiation using green and blue filters and separating the light signal into two channels. The blue channel is mostly contributed by Cerenkov radiation. The W1 Exradin was connected to a two channel SuperMax electrometer (Standard Imaging, Middleton, WI, USA), which collects charges from both channels and eliminates the Cerenkov radiation.[42,43] According to Archambault et al.,[42] this method has been shown to achieve dosimetric accuracy of 0·7% compared to ion chambers. Furthermore, studies showed that perturbation correction factors for plastic and organic scintillators in small fields are close to unity.[44–46] Since these detectors are water equivalent, they match the water mass stopping-power and mass energy absorption coefficient to within ±2% for the range of beam energies in clinical use.[6] Therefore, the electrometer reading in the unit of cGy obtained with the Exradin W1 scintillator gives the absolute dose, and no correction factor needs to be applied.

Measurements in water tank

The 1D Scanner Water Tank (Sun Nuclear, Melbourne, FL, USA) was used for the experimental measurements of PDDs and profiles. PDDs were measured with jaw-defined field sizes of 0·5 × 0·5 cm^2, 1 × 1 cm^2, 2 × 2 cm^2 and 3 × 3 cm^2 for four photons energies: 6 MV,

https://doi.org/10.1017/S1460396919000104 Published online by Cambridge University Press

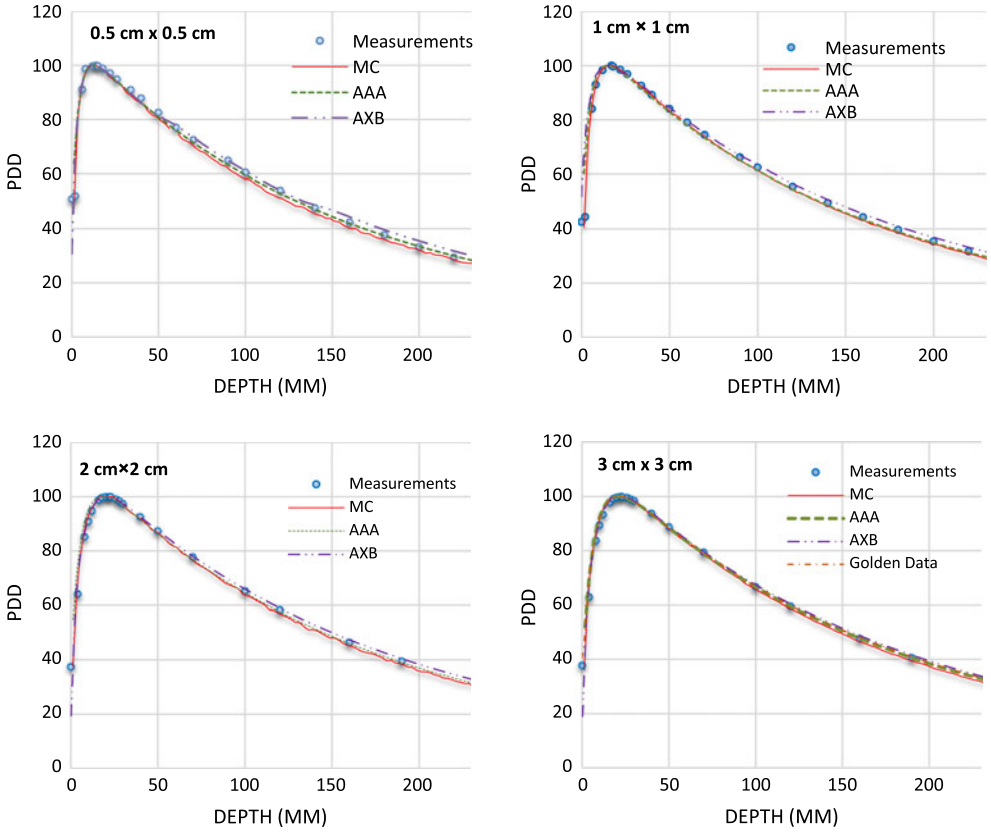


Figure 5. Percentage depth dose (PDD) profiles for 10 FFF MV photon beams with field sizes ranging from 0·5 cm × 0·5 cm to 3 cm × 3 cm in a homogeneous water phantom comparing W1 Exradin scintillator measurements, Monte Carlo (MC) simulations and the calculation algorithms analytical anisotropic algorithm (AAA) and Acuros XB (AXB) in the eclipse treatment planning system. The Varian golden beam data are also included in the plot for a 3 cm × 3 cm field size.

6FFF MV, 10 MV and 10FFF MV, at an SSD of 100 cm. Small fields do not show plateau in the centre of a profile, and therefore determining the exact detector positioning in the centre of the field is challenging; however, the detector was still aligned accurately to the field centre for accurate measurements. To measure the beam profiles, the W1 Exradin was mounted on a computer-controlled IBA Dosimetry (TM) scanning system (RFA300-System, Scanditronix/Wellhofer, Minnesota, USA). In small field measurements, since there is no enough space within the field to place a reference detector, the profile measurements were performed without a reference detector. When measuring in a water tank without a reference detector, it must be assured that the output of the linac is stable with time, for example, by measuring the profile multiple times.[47] Since no reference detector was used for these measurements, we used time-integration or the average of multiple scans to reduce the instantaneous fluctuations. This method is well accepted and, however, can dramatically increase the time needed to acquire scans.

Measurements in solid water

Slabs of solid water phantom (Sun Nuclear Corporation, Melbourne, FL, USA) with dimensions of 30 × 30 × 2 cm^3 were used for all ROF measurements. The slabs were stacked together such that the Exradin W1 scintillator was placed at a depth of 5 cm on the LINAC couch top with an additional 5 cm of solid water phantom underneath the detector for backscatter. The detector was centred in the radiation field and a two channel SuperMax electrometer in the control room was connected to channels 1 and 2 of the W1 Exradin detector, which collects charges from both channels and eliminates the Cerenkov radiation. All the experiments were performed at a dose rate of 600 MU/minute for 6 and 10 MV, 1200 MU/minute for 6FFF MV and 2400 MU/minute for 10FFF MV photon beams at doses of 100 MU and at 100 cm SAD with field sizes ranging from 0·5 × 0·5 cm^2 to 3 × 3 cm^2 defined by the collimator jaws. The output reading of the 10 × 10 cm^2 field was used for normalisation.

Measurements in anthropomorphic head and neck phantom

We investigated the potential use of the W1 Exradin scintillator for patient-specific quality assurance measurements using an anthropomorphic head and neck phantom. We used the stereotactic end-to-end verification (STEEV) head phantom (CIRS, Norfolk, VA, USA) as the anthropomorphic phantom representing the patient for the small field dose measurements. The phantom provides a good approximation of non-homogeneous media present in head and neck (Figure 1a) cases. The phantom was scanned on a SOMATOM Definition AS Open CT simulator (Siemens Healthcare LTD, Oakville, ON, Canada) using institutional protocol for SRS and at 1 mm slice thickness. All the images were then transferred to the Eclipse TPS. Two treatments plans were generated on two different targets at two different locations using institutional protocols. The first target was located in the brain (Figure 1a), whereas the second target was located in the neck region (close to the trachea, Figure 1b). For the brain target, a VMAT treatment plan was generated using two arcs (one full arc and a half vertex arc). The prescription was 2700 cGy in three fractions using 10 FFF MV photon beam without jaw tracking.

https://doi.org/10.1017/S1460396919000104 Published online by Cambridge University Press

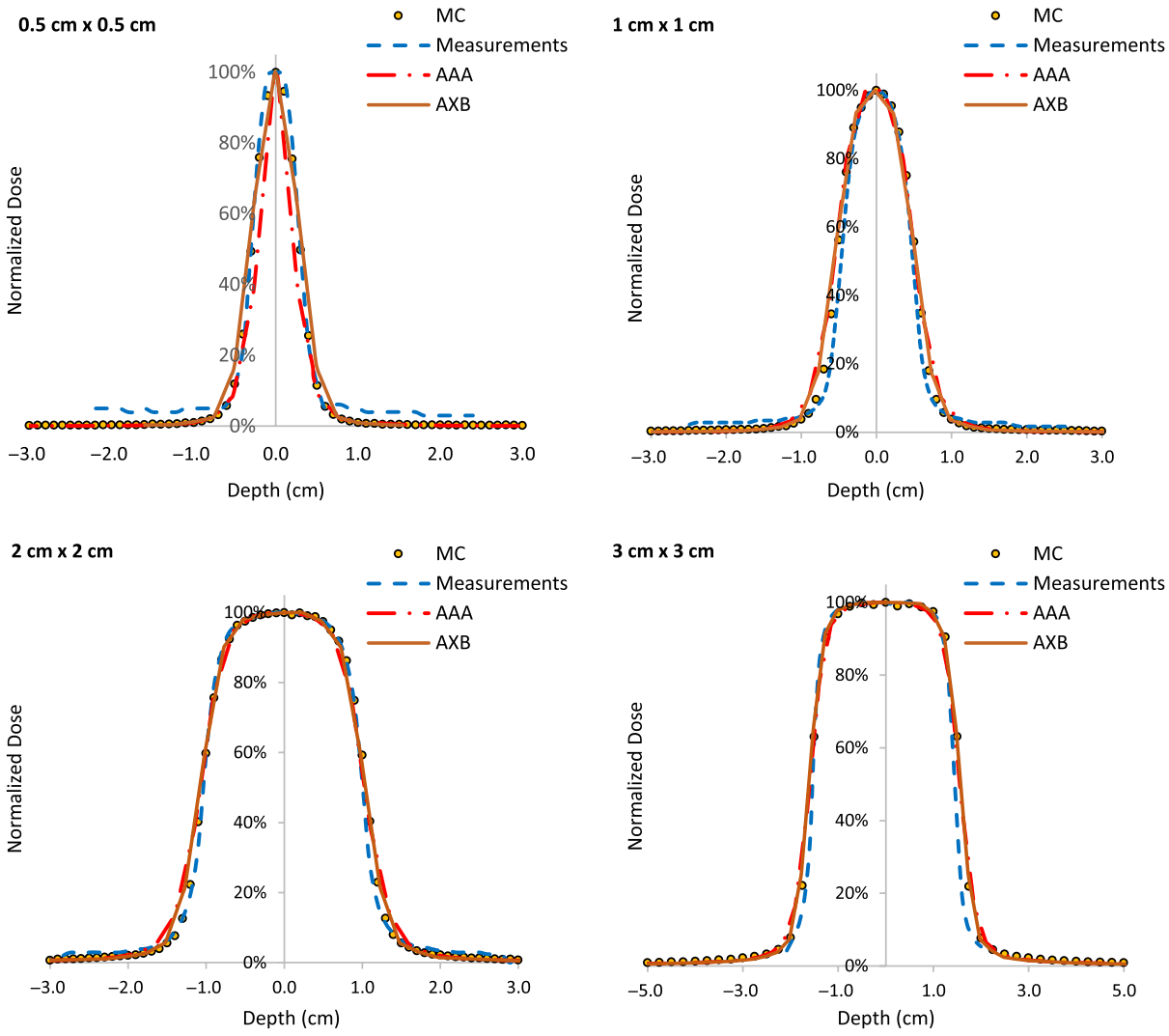


Figure 6. Beam profiles for 6 MV photon beam with field sizes ranging from 0·5 cm × 0·5 cm to 3 cm × 3 cm in a homogeneous water phantom comparing W1 Exradin scintillator measurements, the calculation algorithms analytical anisotropic algorithm (AAA) and Acuros XB (AXB) in the eclipse treatment planning system and Monte Carlo (MC) simulated data.

For the neck target, two full arcs, clockwise and counter clockwise, were used to deliver a prescribed dose was 5000 cGy in 25 fractions using 6 MV photon beam. Two predrilled cylindrical holes in the neck of the phantom provided access for the scintillator to be positioned in the targets. At the treatment unit, cone beam CT was used to accurately position the phantom to ensure that the targets are aligned correctly to the radiation field portals. All treatment deliveries were accomplished on a Varian TrueBeam Linear accelerator.

Results

PDDs for 0·5 × 0·5 cm^2, 1 × 1 cm^2, 2 × 2 cm^2 and 3 × 3 cm^2 field sizes and for 6 MV, 6FFF MV, 10 MV and 10FFF MV photon beam energies are shown in Figures 2–5. The Varian GBD for a 3 × 3 cm^2 field size is also shown in Figures 2–5. Figures 6 and 7 show beam profiles measured for 6 MV and 6FFF MV photon beams respectively at a depth of 5 cm comparing MC simulation, measurements and the AAA and AXB calculation algorithms. For the 6 MV photon, the FWHM values derived from MC, W1 Exradin measurements, AAA and AXB profiles are 0·61, 0·51, 0·64 and 0·64 cm for the 0·5 × 0·5 cm^2 field size; 1·01, 0·97, 1·15 and 1·15 cm for the 1 × 1 cm^2 field size; 2·1, 2, 2·06 and 2·06 cm for the 2 × 2 cm^2 field size; and 3·12, 3·0, 3·12 and 3·12 cm for the 3 × 3 cm^2 field size, respectively. Similarly, for the 6FFF MV photon, the FWHM values derived from MC, W1 Exradin measurements, AAA and AXB profiles are 0·60, 0·60, 0·44 and 0·68 cm for the 0·5 × 0·5 cm^2 field size; 1·08, 1·01, 0·85 and 1·10 cm for the 1 × 1 cm^2 field size; 2·1, 2, 2·1 and 2·11 cm for the 2 × 2 cm^2 field size; and 3·02, 3·0, 3·04 and 3·16 cm for the 3 × 3 cm^2 field size, respectively.

Table 1 shows the PDD results at depths of 5, 10 and 20 cm comparing MC simulated data, measured data with the W1 Exradin detector and calculated data from the eclipse TPS with both AAA and AXB calculation algorithms. The data show good agreement between the W1 Exradin measurements and the MC simulation data. Data in Table 1 show that the difference of the PDDs between AAA and measurements averaged over all the energies is 6·6, 1·7, 0·7 and 1·2 at the depth of 5 cm; 4·4, 2·0, 1·2 and 1·2 at the depth of 10 cm; and 5·5, 2·5, 0·5 and 1·2 at the depth of 20 cm for field sizes of 0·5 × 0·5 cm^2, 1 × 1 cm^2, 2 × 2 cm^2 and 3 × 3 cm^2, respectively. Similarly, the difference between AXB and measurements averaged over all beam energies is calculated to be 4·6, 0·2, 1·6 and 1·9 at the depth of 5 cm; 3·2, 1·6, 2·8 and 2·1 at the depth of

https://doi.org/10.1017/S1460396919000104 Published online by Cambridge University Press

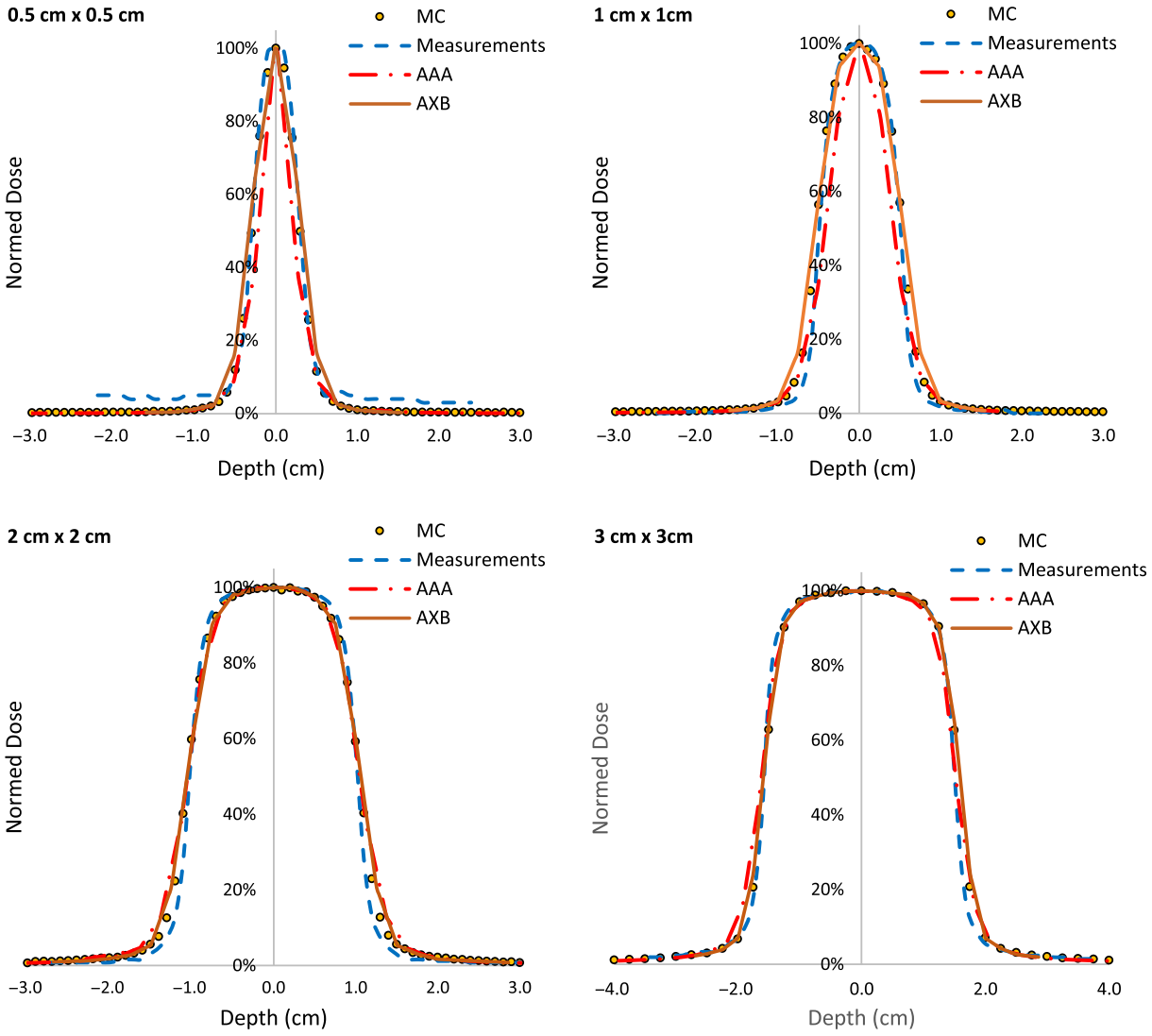


Figure 7. Beam profiles for 6FFF MV photon beam with field sizes ranging from 0·5 cm × 0·5 cm to 3 cm × 3 cm in a homogeneous water phantom comparing W1 Exradin scintillator measurements, the calculation algorithms analytical anisotropic algorithm (AAA) and Acuros XB (AXB) in the eclipse treatment planning system and Monte Carlo (MC) simulated data.

10 cm; and 8·2, 4·8, 4·1 and 3·3 at the depth of 20 cm for field sizes of 0·5 × 0·5 cm^2, 1 × 1 cm^2, 2 × 2 cm^2 and 3 × 3 cm^2, respectively. ROFs from measurements and TPS calculations using AAA and AXB are tabulated in Table 2 for different beam energies and field sizes. Compared with the W1 Exradin measurements, the ROF values are underestimated by the AAA algorithm, averaged over all the energies by 9·9, 2·4, 1·4 and 0·7% for field sizes of 0·5 × 0·5 cm^2, 1 × 1 cm^2, 2 × 2 cm^2 and 3 × 3 cm^2, respectively. Similarly, the ROF values are overestimated by the AXB algorithm, averaged over all the energies by 1·3 and 1·6% for 0·5 × 0·5 cm^2 and 1 × 1 cm^2 field sizes and underestimated by 0·3 and 0·9% for 2 × 2 cm^2 and 3 × 3 cm^2 field sizes, respectively. In general, the AXB algorithm is in good agreement with measurements for small fields than the AAA algorithm.

Table 3 shows the comparison of isocenter point doses for MC simulation, W1 Exradin measurement and AAA and AXB TPS calculation algorithms at the centre of different brain target sizes in the STEEV phantom (Figure 1a). The target sizes ranged from 0·5 to 3 cm^3. For the 0·5 cm^3 target size, results from the MC simulation, doses calculated by Eclipse AAA and AXB algorithms are about 1·5, 4·3 and 1·3% higher than dose measured by W1 Exradin, respectively. For the 1 cm^3 target size, doses simulated by MC and calculated by Eclipse AAA and AXB algorithms are 3·3, 2·7 and 4·5% higher than that measured by W1 Exradin, respectively. For the 2 cm^3 target, MC simulation, AAA and AXB show dose difference of −2·2, 4·0 and 3·4%, respectively, compared to W1 Exradin measurements, and similarly, for the 3 cm^3 target the MC simulation, AAA and AXB show dose difference of −1·8, 2·1 and 1·6%, respectively, compared to measurements. Table 4 shows the point doses at the centre of the target located at the neck region close to the trachea (Figure 4b) using MC simulation, W1 Exradin measurements and AAA and AXB TPS calculated dose. For the 0·5 cm^3 target size, the dose simulated by MC and calculated by TPS AAA and AXB are about 0·9, 4·3 and −1·9% different from measurements, respectively. For the 1 cm^3 target size, doses simulated by MC and calculated by Eclipse AAA and AXB algorithms vary by about −4·6, 5·6 and 5·1% compared to measurements, respectively. For the 2 cm^3 target, MC simulation, AAA and AXB show dose differences of 4·9, 6·5 and 5·4%, respectively, compared to measurements and similarly for the 3 cm^3 target, the

https://doi.org/10.1017/S1460396919000104 Published online by Cambridge University Press

Table 1. Percentage depth dose values acquired at different depths comparing Monte Carlo simulated data, measured data with the W1 Exradin detector and calculated data from the eclipse TPS with both the analytical anisotropic algorithm (AAA) and Acuros XB (AXB) calculation algorithms for different field sizes and photon beam energies

Photon energy (MV)	Depth (cm)	Percentage depth doses													
		MC simulation (%)				Measurements with W1 Exradin (%)				AAA (%)				AXB (%)			
		0·5x0·5 cm^2	1x1 cm^2	2x2 cm^2	3x3 cm^2	0·5 × 0·5 cm^2	1 × 1 cm^2	2 × 2 cm^2	3x3 cm^2	0·5 × 0·5 cm^2	1 × 1 cm^2	2 × 2 cm^2	3x3 cm^2	0·5 × 0·5 cm^2	1 × 1 cm^2	2 × 2 cm^2	3x3 cm^2
6X	5	67·0	78·9	80·9	82·2	66·5	78·3	81·8	82·9	77·8	78·9	80·6	82·7	78·2	79·5	84·5	85·7
	10	53·5	55·5	57·9	59·5	53·7	55·9	59·3	60·8	55·9	56·7	58·3	60·4	56·4	57·6	61·6	62·7
	20	27·1	29·3	30·2	31·0	27·2	28·5	31·7	32·8	29·3	30·0	30·9	32·2	30·5	31·2	33·3	33·1
6FFF	5	73·5	75·8	78·7	79·7	71·6	76·5	79·5	80·8	75·8	77·0	79·1	80·6	74·6	76·3	82·1	84·0
	10	49·3	51·5	54·3	55·9	48·1	52·7	54·6	57·2	52·0	53·3	55·3	56·9	51·9	53·5	58·0	59·6
	20	23·9	26·0	27·5	28·0	22·9	26·4	28·3	29·2	25·1	26·6	27·8	28·8	26·1	27·5	29·9	30·9
10X	5	84·0	86·0	88·9	89·7	85·1	86·5	89·3	90·4	89·5	90·3	92·0	92·9	85·1	86·5	89·5	90·9
	10	63·2	63·6	68·2	69·5	63·9	65·6	68·5	69·7	68·5	69·0	70·8	72·0	65·3	66·6	69·1	70·4
	20	37·6	37·6	40·5	41·8	38·1	39·4	40·1	41·6	40·2	41·0	42·2	43·1	39·6	40·4	41·7	42·6
10FFF	5	80·3	83·2	86·6	88·1	82·6	84·0	87·4	88·8	81·2	84·8	89·1	90·9	79·7	83·7	86·9	88·4
	10	58·3	61·2	63·8	65·8	60·6	62·3	65·3	66·8	59·4	62·5	66·5	68·5	59·1	62·6	65·5	66·9
	20	32·2	34·3	35·9	37·4	33·2	35·3	37·6	37·7	32·9	35·3	38·0	39·4	34·1	36·4	38·2	39·2

Table 2. Relative output factors (ROFs) comparing calculated data using both analytical anisotropic algorithm (AAA) and Acuros XB (AXB) algorithms against measurements using the W1 Exradin detector. %diff is calculated for eclipse AAA and AXB with respect to W1 Exradin scintillator measurement

Photon energy (MV)	Field size (cm^2)	Measurement Exradin W1 Scintillator	Eclipse AAA		Eclipse AXB	
		ROF	ROF	% diff	ROF	% diff
6X	0·5 × 0·5	0·418	0·378	−9·6	0·427	2·1
	1 × 1	0·720	0·707	−1·8	0·738	2·4
	2 × 2	0·852	0·843	−1·1	0·850	−0·3
	3 × 3	0·887	0·881	−0·7	0·878	−1·0
	10 × 10	1·000	1·000	0·0	1·000	0·0
6FFF	0·5 × 0·5	0·452	0·405	−10·4	0·458	1·4
	1 × 1	0·755	0·739	−2·1	0·763	1·1
	2 × 2	0·867	0·859	−0·9	0·865	−0·2
	3 × 3	0·902	0·896	−0·6	0·894	−0·9
	10 × 10	1·000	1·000	0·0	1·000	0·0
10X	0·5 × 0·5	0·356	0·317	−10·9	0·358	0·4
	1 × 1	0·649	0·630	−3·0	0·663	2·1
	2 × 2	0·839	0·822	−2·0	0·836	−0·4
	3 × 3	0·894	0·884	−1·1	0·883	−1·2
	10 × 10	1·000	1·000	0·0	1·000	0·0
10FFF	0·5 × 0·5	0·393	0·358	−8·9	0·398	1·3
	1 × 1	0·706	0·687	−2·7	0·712	0·9
	2 × 2	0·877	0·864	−1·5	0·874	−0·4
	3 × 3	0·925	0·922	−0·3	0·920	−0·5
	10 × 10	1·000	1·000	0·0	1·000	0·0

MC simulation, AAA and AXB show dose differences of 4·9, 6·5 and 5·4%, respectively, compared to measurements. In general, the MC simulation and AXB show good agreement with measurement for small fields' measurements in the anthropomorphic head phantom.

Discussions

In modern radiation therapy, recent technological advances in dose delivery, patients positioning, target localisation and immobilisation of patients have led to more complex treatment planning such as SRS and SBRT. In these techniques, small field sizes are often used to treat small target volumes and minimising doses to surrounding normal tissues. Consequently, it becomes necessary to be able to determine the dose in small photon beams with high accuracy, both in TPS commissioning and patient-specific quality assurance. However, the lateral electron disequilibrium, the finite size of the detectors and the non-water equivalence of the materials make the accuracy of small-field dosimetry challenging. Many publications have been concerned with the validation and comparison of the AXB algorithm against measurements, MC simulations, AAA algorithms or a combination of these modalities in small fields.[47–49] Stathakis et al.[31] investigated the accuracy of small field dosimetry using the AXB dose calculation algorithm in homogenous and heterogenous media. They concluded that in a

https://doi.org/10.1017/S1460396919000104 Published online by Cambridge University Press

Table 3. Comparison of isocenter point doses for MC simulation, W1 Exradin measurement and the analytical anisotropic algorithm (AAA) and Acuros XB (AXB) TPS calculation algorithms at the centre of different brain target sizes of the anthropomorphic head and neck phantom. The beam energy used for the treatment planning and delivery is 10FFF MV

Target size (cm^3)	Fixed jaw size (cm^2)	Dose (cGy)						
		Monte Carlo simulation		W1 Exradin measurement	Eclipse AAA		Eclipse AXB	
		Dose	%diff*		Dose	%diff*	Dose	%diff*
0·5	1·4 × 2	902	1·5	889	927	4·3	901	1·3
1	2 × 2	927	3·3	897	921	2·7	937	4·5
2	2·8 × 2·8	830	−2·2	849	883	4·0	878	3·4
3	4 × 4	850	−1·8	866	884	2·1	880	1·6

*The differences (%diff) were found with W1 Exradin measurements.

Table 4. Comparison of isocenter point doses for MC simulation, W1 Exradin measurement and the analytical anisotropic algorithm (AAA) and Acuros XB (AXB) TPS calculation algorithms at the centre of different neck target (close to trachea) sizes of the anthropomorphic head and neck phantom. The beam energy used for the treatment planning and delivery is 6 MV

Target size (cm^3)	Fixed jaw size (cm^2)	Dose (cGy)						
		Monte Carlo simulation		W1 Exradin measurement	Eclipse AAA		Eclipse AXB	
		Dose	%diff*		Dose	%diff*	Dose	%diff*
0·5	1·4 × 2	213	0·9	211	220	4·3	207	−1·9
1	2 × 2	204	4·6	195	206	5·6	205	5·1
2	2·8 × 2·8	193	4·9	184	196	6·5	194	5·4
3	4 × 4	194	4·9	185	197	6·5	195	5·4

*The differences (%diff) were found with W1 Exradin measurements.

homogeneous phantom, the AAA and AXB showed good agreement with MC simulations. However, when dose calculations in heterogenous phantoms were compared to MC simulations, the AXB had better agreement than AAA. Qin et al.[33] evaluated plastic scintillator dose measurements for small field stereotactic patient-specific quality assurance. They concluded that the Exradin detector demonstrated superior performances in plans with small fields and heavy modulation, and thus the Exradin is a suitable detector for clinical routine SRS quality assurance dose measurements. Fogliata et al.[49] evaluated the dose calculation accuracy for small fields defined by jaws or MLCs using the AAA and AXB algorithms. They used single point output factor measurement using a PTW microDiamond detector for 6 MV, 6FFF MV and 10FFF MV beams with a Varian TrueBeam. Measurements were compared with the AAA and AXB dose calculation algorithms. They found an agreement of less than 0·5% for field sizes as small as 2 × 2 cm^2. For smaller fields, both algorithms either overestimated the dose for jaw-defined field sizes or underestimated the dose for MLC-defined field sizes. In the very small field region (as small as 0·5 × 0·5 cm^2), the AXB achieved agreement within 3% with measurements. In this study, we observed that the AXB showed good agreement of about 0·3% with Exradin measurements, whereas the AAA showed a relative difference of 2·9% (Table 2). The AAA algorithm shows dose underestimation of about 10·9% for field sizes as small as 0·5 × 0·5 cm^2 with the 10 MV beam. The AXB algorithm shows dose underestimation of less than 1% for 2 × 2 cm^2 and 3 × 3 cm^2 field sizes and dose overestimation of less than 2·5% for 0·5 × 0·5 cm^2 and 1 × 1 cm^2 field sizes (Table 2).

Godson et al.[34] investigated the depth of dose maximum (D_{max}) and depth dose at 10 cm (DD_{10}) with different detectors including cylindrical ion chamber, shielded diode, unshielded diode and parallel plate ion chamber. They used small field sizes of 1 × 1 cm^2, 2 × 2 cm^2 and 3 × 3 cm^2 using a Varian linear accelerator with 6 MV photon beam. They reported the biggest detector-to-detector variation for DD_{10} for the 1 × 1 cm^2 and negligible deviation was found for larger fields. For 1 × 1 cm^2 field size, they reported DD_{10} minimum and maximum values of about 57% (using shielded diode) and 60% (using parallel plate ion chamber), respectively. In this study, we measured DD_{10} of 55·9% for 6 MV photon beam and 1 × 1 cm^2 field size, which agrees well with the shielded diode measurement. Also, the DD_{10} with shielded diode measurement by Gordon et al.[34] of 59 and 61% for the field sizes of 2 × 2 cm^2 and 3 × 3 cm^2, respectively, agrees well with the W1 Exradin measurement of DD_{10} of 59·3 and 60·8% in our study. Pasquino et al.[35] investigated dosimetric characterisation in small X-ray fields using a microchamber and a plastic scintillator detector. They measured PDDs for 1 × 1 cm^2, 2 × 2 cm^2 and 3 × 3 cm^2 field size for 6 MV photon beam and acquired DD% at depths 5 cm, 10 cm and 20 cm. They concluded that both micro-ion chamber (A26 IC) and W1 Exradin could play an important role in small field relative dosimetry. Our measurements for 6 MV photon beam agreed well with their results. AAA and AXB beam profile and PDD results were not very different in a homogeneous medium. However, in the presence of heterogeneity, our results confirmed that AXB presents closer agreement with measured values compared to AAA (Tables 3 and 4). The results in Tables 3 and 4 showed that the average dose difference between measurements and MC

https://doi.org/10.1017/S1460396919000104 Published online by Cambridge University Press

simulation is 0·2 and 3·8% for the tumours located in the brain and neck region, respectively.

There are some limitations that may be associated with the measurements, simulations and TPS calculations when dealing with small fields such as the accurate positioning of the detector for measurement, accurate material composition for AXB algorithm and noise in MC simulations for small voxel size. Although we attempted to position the detector at the centre of the tumours and also aligned the detector correctly to the field centre for accurate measurements of PDDs, profiles and ROFs, determining the exact detector positioning in the centre of the field is still a challenge. Also since the AXB algorithm uses the material composition for the voxels from a predefined material library for dose calculations, accurate material composition data for each voxel are important for accurate dosimetry.

Conclusions

We have investigated the accuracy of AXB algorithm and the AAA in small fields against W1 Exradin and MC techniques. We made the comparison of dosimetric parameters including PDDs, beam profile and ROFs in water phantom. We observed that the W1 Exradin measurements agree well with MC simulation in both homogeneous medium and heterogeneous anthropomorphic phantom medium representing a patient. Therefore, W1 Exradin can be used efficiently to measure dosimetric parameters in small fields and for patient-specific quality assurance measurements. In both homogenous and heterogeneous media, the AXB algorithm dose prediction agrees well with both measurements and MC simulation and was found to be superior to the AAA algorithm.

Author ORCIDs. Ernest Osei 0000-0002-4114-3273

Acknowledgements. The author Sepideh Behinaein would like to acknowledge with gratitude the support received from all the Medical Physicists, Electronic Technologists, Medical Physics Associate, Radiation Therapists and Radiation Oncologists in the Radiation Oncology Program at the Grand River Regional Cancer Centre during the time of residency at the Medical Physics Department.

References

1. Sharma S D. Challenges of small photon field dosimetry are still challenging. J Med Phys 2014; 39: 131–132.
2. Aspradakis M, Byrne J, Palmans H et al. Small field MV photon dosimetry. IPEM Report No. 103. York, UK: Institute of Physics and Engineering in Medicine, 2010.
3. Das I J, Ding G X, Ahnesjö A. Small field: nonequilibrium radiation dosimetry. Med Phys 2008; 35: 206–215.
4. Massillon-J L G. Dosimetry in steep dose-rate gradient radiation fields: a challenge in clinical applications. Eleventh Mexican Symposium on Medical Physics AIP Conference Proceeding, Mexico City, (Mexico). 2010; 1310: 23–28.
5. Alfonso R, Andreo P, Capote R et al. A new formalism for reference dosimetry of small and nonstandard fields. Med Phys 2008; 35: 5179–5186.
6. International Atomic Energy Agency. Dosimetry of Small Static Fields Used in External Beam Radiotherapy. Technical Reports Series No. 483, IAEA, Vienna. 2017: 1–211.
7. Carrasco P, Jornet N, Jordi O et al. Characterization of the Exradin W1 scintillator for use in radiotherapy. Med Phys 2014; 42: 297–304.
8. Laub WU, Wong T. The volume effect of detectors in the dosimetry of small fields used in IMRT. Med Phys 2003; 30: 341–347.
9. Le Roy M, De Carlan L, Delaunay F et al. Assessment of small volume ionization chambers as reference dosimeters in high-energy photon beams. Phys Med Biol 2011; 56: 5637–5650.
10. Andersson J, Kaiser F J, Gómez F et al. A comparison of different experimental methods for general recombination correction for liquid ionization chambers. Phys Med Biol 2012; 57: 7161–7175.
11. Pardo-Montero J, Gómez F. Determining charge collection efficiency in parallel-plate liquid ionization chambers. Phys Med Biol 2009; 54: 3677–3689.
12. Chung E, Davis S, Seuntjens J. Experimental analysis of general ion recombination in a liquid-filled ionization chamber in high-energy photon beams. Med Phys 2013; 40 (6): 062104-1–7.
13. Eklund K. Modeling silicon diode dose response in radiotherapy fields using fluence pencil kernels, PhD Thesis, Uppsala University (2010).
14. Scott A J, Kumar S, Nahum A E, Fenwick J D. Characterizing the influence of detector density on dosimeter response in non-equilibrium small photon fields. Phys Med Biol 2012; 57: 4461–4476.
15. Gagnon J C, Thériault D, Guillot M et al. Dosimetric performance and array assessment of plastic scintillation detectors for stereotactic radiosurgery quality assurance. Med Phys 2012; 39: 429–436.
16. Francescon P, Cora S, Cavedon C et al. Use of a new type of radiochromic film, a new parallel-plate micro-chamber, MOSFETs, and TLD 800 microcubes in the dosimetry of small beams. Med Phys 1998; 125: 503–511.
17. Alnawaf H, Buston M J, Cheuung T et al. Scanning orientation and polarization effects for XRQA radiochromic film. Phys Med 2010; 26: 216–219.
18. Ramani R, Russell S, O'Brien P. Clinical dosimetry using MOSFETs. Int J Radiat Oncol Biol Phys 1997; 37: 959–964.
19. Jursinic P A. Characterization of optically stimulated luminescent dosimeters, OSLDs, for clinical dosimetric measurements. Med Phys 2007; 34: 4594–4604.
20. Fogliata A, Cozzi L. Dose calculation algorithm accuracy for small fields in non-homogeneous media: the lung SBRT case. Phys Med 2017; 44: 157–162.
21. Cassell K J, Hobday P A, Parker R P. The implementation of a generalized Batho inhomogeneity correction for radiotherapy planning with direct use of CT numbers. Phys Med Biol 1981; 26: 825–833.
22. Sontag M R, Cunningham J R. The equivalent tissue-air ratio method for making absorbed dose calculations in a heterogeneous medium. Radiology 1978; 129: 787–794.
23. Engelsman M, Damen E M, Koken P W et al. Impact of simple tissue inhomogeneity correction algorithms on conformal radiotherapy of lung tumours. Radiother Oncol 2001; 60: 299–309.
24. Tillikainen L, Helminen H, Torsti T et al. A 3D pencil-beam-based superposition algorithm for photon dose calculation in heterogeneous media. Phys Med Biol 2008; 53: 3821–3839.
25. Ahnesjö A, Andreo P, Brahme A. Calculation and application of point spread functions for treatment planning with high energy photon beams. Acta Oncol 1987; 26: 49–56.
26. Vassiliev O N, Wareing T A, McGhee J et al. Validation of a new grid-based Boltzmann equation solver for dose calculation in radiotherapy with photon beams. Phys Med Biol 2010; 55: 581–598.
27. Han T, Mikell J K, Salehpour M, Mourtada F. Dosimetric comparison of Acuros XB deterministic radiation transport method with Monte Carlo and model-based convolution methods in heterogeneous media. Med Phys 2011; 38 (5): 2651–2664.
28. Fogliata A, Vanetti E, Albers D et al. On the dosimetric behaviour of photon dose calculation algorithms in the presence of simple geometric heterogeneities: comparison with Monte Carlo calculations. Phys Med Bio 2007; 52: 1363–1385.
29. Hasenbalg F, Neuenschwander H, Mini R, Born E J. Collapsed cone convolution and analytical anisotropic algorithm dose calculations compared to VMC++ Monte Carlo simulations in clinical cases. Phys Med Biol 2007; 52: 3679–3691.
30. Hoffmann L, Alber M, Söhn M, Elstrøm U V. Validation of the Acuros XB dose calculation algorithm versus Monte Carlo for clinical treatment plans. Med Phys 2018; 45: 3909–3915.

https://doi.org/10.1017/S1460396919000104 Published online by Cambridge University Press

31. Stathakis S, Esquivel C, Quino L V. Accuracy of the small field dosimetry using the Acuros XB dose calculation algorithm within and beyond heterogeneous media for 6 MV photon beams. Int J Med Phys Clin Eng Radiat Oncol 2012; 1: 78–87.
32. Zavan R, McGeachy P, Madamesila J et al. Verification of Acuros XB dose algorithm using 3D printed low-density phantoms for clinical photon beams. J Appl Clin Med Phys 2018; 19: 32–43.
33. Qin Y, Gardner S J, Kim J et al. Technical Note: evaluation of plastic scintillator detector for small field stereotactic patient-specific quality assurance. Med Phys 2017; 44: 5509–5516.
34. Godson H F, Ravikumar M, Sathiyan S et al. Analysis of small field percent depth dose and profiles: comparison of measurements with various detectors and effects of detector orientation with different jaw settings. Med Phys 2016; 41: 12–20.
35. Pasquino M, Cutaia C, Radici L et al. Dosimetric characterization and behaviour in small X-ray fields of a microchamber and a plastic scintillator detector. Br Radiol 2017; 90: 20160596, 1–8.
36. Das I J, Cheng C, Watts R J et al. Accelerator beam data commissioning equipment and procedures: report of the TG-106 of the Therapy Physics Committee of the AAPM. Med Phys 2008; 35: 4186–4214.
37. Hoffmann L, Jørgensen M B, Muren L P, Petersen J B. Clinical validation of the Acuros XB photon dose calculation algorithm, a grid-based Boltzmann equation solver. Acta Oncol 2012; 51 (3): 376–385.
38. Fogliata A, Nicolini G, Clivio A, Vanetti E, Cozzi L. Accuracy of Acuros XB and AAA dose calculation for small fields with reference to RapidArc(®) stereotactic treatments. Med Phys 2011; 38(11): 6228–6237.
39. Lobo J, Popescu I. Two new DOSXYZnrc sources for 4D Monte Carlo simulations of continuously variable beam configurations, with applications to RapidArc, VMAT, TomoTherapy and CyberKnife. Phy Med Biol 2010; 55 (16): 4431–4474.
40. Mackie T R, Khatib E, Battista J et al. Lung dose corrections for 6- and 15-MV x rays. Med Phys 1985; 12: 327–332.
41. White D R, Booz J, Griffith R et al. Tissue substitutes in radiation dosimetry and measurement (Report 44). J Int Commission Radiat Units Meas 1989: 23 (1): 1–189.
42. Archambault L, Beddar A S, Gingras L et al. Measurement accuracy and Cerenkov removal for high performance, high spatial resolution scintillation dosimetry. Med Phys 2006; 33: 128–135.
43. Guillot M, Gingras L, Archambault L et al. Spectral method for the correction of the Cerenkov light effect in plastic scintillation detectors: a comparison study of calibration procedures and validation in Cerenkov light-dominated situations. Med Phys 2011; 38: 2140–2150.
44. Ralston A, Liu P, Warrener K et al. Small field diode correction factors derived using an air core fiber optic scintillation dosimeter and EBT2 film. Phys Med Biol 2012; 57: 2587–2602.
45. Azangwe G, Grochowska P, Georg D et al. Detector to detector corrections: a comprehensive experimental study of detector specific correction factors for beam output measurements for small radiotherapy beams. Med Phys 2014; 41: 072103-1–16.
46. Wuerfel J U. Dose measurements in small fields. Med Phy Int J 2013; 1: 81–90.
47. Zhen H, Hrycushko B, Lee H et al. Dosimetric comparison of Acuros XB with collapsed cone convolution/superposition and anisotropic analytic algorithm for stereotactic ablative radiotherapy of thoracic spinal metastases. J Appl Clin Med Phy 2015; 16: 181–192.
48. Hirata K, Nakamura M, Yoshimura M et al. Dosimetric evaluation of the Acuros XB algorithm for a 4MV photon beam in head and neck intensity-modulated radiation therapy. J Appl Clin Med Phy 2015; 16: 52–64.
49. Fogliata A, Lobefalo F, Reggiori G et al. Evaluation of the dose calculation accuracy for small fields defined by jaw or MLC for AAA and Acuros XB algorithms. Med Phys 2016; 43(10): 5685–5694.

https://doi.org/10.1017/S1460396919000104 Published online by Cambridge University Press